Monolayers of Biphenyl-3,4',5-tricarboxylic Acid Formed on Cu and Ag from Solution

Hannah Aitchison, [a] *Hao Lu,* [b,†] *Michael Zharnikov* [b] *and Manfred Buck* *[a]

[a] EaStCHEM School of Chemistry, University of St Andrews, North Haugh, St Andrews KY16 9ST, United Kingdom.

[b] Angewandte Physikalische Chemie, Universität Heidelberg, Im Neuenheimer Feld 253, 69120 Heidelberg, Germany.

* Fax: +441334 463808; Tel: 441334463800; E-mail: mb45@st-andrews.ac.uk

† Present address: Max Planck Institute for Polymer Research, Ackermannweg 10, 55128 Mainz, Germany.

ABSTRACT

Self-assembled monolayers of biphenyl-3,4',5-tricarboxylic acid (BPTCA) on Au(111)/mica substrates modified by under-potential deposited layers of Cu and Ag were studied by scanning tunneling microscopy under ambient conditions as well as by synchrotron based X-ray photoelectron spectroscopy and near-edge X-ray absorption fine structure spectroscopy. BPTCA forms distinctly different layers on Ag and Cu due to a pronounced influence of the substrate on the balance of intermolecular and molecule-substrate interactions. On Cu a highly crystalline commensurate row structure is formed, described by a $6\times\sqrt{3}$ unit cell, a molecular tilt of 45-50° relative to the surface normal, and a bipodal bidentate adsorption geometry. In contrast, incommensurate row structures are formed on Ag which are characterized by significant waves and kinks, a monopodal bidentate adsorption geometry, and a tilt angle of 25-30°. While BPTCA parallels its smaller homologue, benzene-1,3,5-tricarboxylic acid, with regard to the substrate specific monopodal and bipodal adsorption geometries, the preparation conditions for the monolayer on Cu and the film structure on Ag are pronouncedly different. The results are discussed in terms of the steric requirements and molecular symmetry of BPTCA.

INTRODUCTION

Aromatic carboxylic acids are widely used components of supramolecular self-assembled systems, in particular of 3D metal-organic frameworks (MOFs) where they constitute versatile organic linkers.[1] On solid supports they have been investigated as building blocks for 2D supramolecular networks, where the plane of the aromatic system is orientated parallel to the surface.[2-5] In contrast, studies on the assembly of such molecules on solid supports in a non-flat adsorption geometry are scarce even though this is of interest for accessing the third dimension, as in the layer-by-layer growth of thin film MOFs from a modified surface (SURMOFs) where carboxylic acid moieties provide convenient coordination points for metals.[6-8]

The 2D self-assembly of molecules of aromatic carboxylic acids in plane with the substrate has been investigated in great detail under ultra-high vacuum (UHV) conditions mainly on metal surfaces such as Au, Ag and Cu[2-5] but more recently also on non-metallic surfaces such as TiO_2 [9] and $CaCO_3$.[10] On metals instances of deprotonation of the carboxylic acid group have been reported on more reactive surfaces such as Cu[11-18] or Pd[19]. However, for deprotonation to occur on an inert surface such as Au or Ag, an additional driving force is usually required, for example elevated temperatures[20-22] or the presence of promoting metal adatoms such as Cu or Fe.[23-27] When deprotonation does occur, either the molecules maintain a flat-lying geometry or undergo a transition to an upright orientation with the bonding to the surface through a COO^- group,[12-14, 16] thus, resulting in a coexistence of upright and flat-lying molecules.

In comparison to UHV, there are fewer reports of aromatic carboxylic acids adsorbed on a surface from solution-based processing. Like in UHV, the focus has been on in-plane structures[28-38] with structural motifs based on benzene-1,3-dicarboxylic acid (isophthalic acid, IPA), benzene-1,3,5-tricarboxylic acid (trimesic acid, TMA) and higher homologues being of

particular interest due to their ability to form extended networks and/or exhibiting random tilings and analogies to glasses. Studies of layers where molecules adopt an upright orientation and exhibit a dense packing are scarce and only comprise alkoxy substituted aromatic monocarboxylic acids[39-40] as well as IPA and TMA.[41-43] In these cases reactive substrates such as Ag and Cu were used, which the molecules bind to via carboxylate-metal coordination bonding. On less reactive surfaces such as gold, an upright orientation can be achieved under an electrochemical environment when sufficient positive potential is applied to a Au electrode to induce deprotonation of the carboxylic acid moiety.[44-47]

A comparative study of TMA on Au(111)/mica substrates, modified by underpotential deposited (UPD) Cu and Ag layers, revealed fundamental differences in the film structures for the two substrates.[41] The pronounced influence of the substrate on the balance of intermolecular and molecule-substrate interactions gives rise to an inversion of the molecular orientation, which is reflected by a bipodal and monopodal adsorption geometry on Cu and Ag, respectively. To advance our understanding of the self-assembly of aromatic carboxylic acids at the liquid/solid interface, biphenyl-3,4',5-tricarboxylic acid (BPTCA, Scheme 1), an analogue of TMA, was investigated. This compound has been of interest for metal-organic frameworks (MOFs)[48-55] where the unsymmetrical substitution pattern yields an unusual structure, combining different coordination bonding motifs[48]. On surfaces like those of Cu and Ag it is anticipated from our study of TMA[41] that BPTCA can coordinatively bind in either a bipodal or monopodal fashion depending on whether the isophthalic or benzoic acid part of the molecule faces the substrate. However, it is not clear *a priori* how, as compared to TMA, the additional benzene ring affects the assembly kinetics and energetics of the layer, and whether the lower symmetry of the molecule gives rise to changes in the adsorption geometry.

To address these questions we studied the solution-based self-assembly of BPTCA on Au(111)/mica substrates modified by UPD layers of copper and silver using a combination of microscopy and advanced X-ray spectroscopies.

Scheme 1. Structures of biphenyl-3,4',5-tricarboxylic acid (BPTCA) investigated in this study and related molecules, benzoic acid (BA), isophthalic acid (IPA) and trimesic acid (TMA).

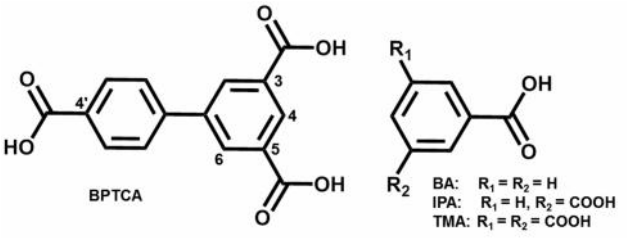

EXPERIMENTAL METHODS

Sample Preparation.

Materials. Biphenyl-3,4',5-tricarboxylic acid (96%, Sigma-Aldrich), $AgNO_3$ (99.9999%, Sigma-Aldrich), HNO_3 (70%, 99.999+% purity, Sigma-Aldrich), $CuSO_4 \cdot 5H_2O$ (99.999%, Sigma-Aldrich), KCl (≥99.5%, Fluka) and ethanol (AnalaR Normapur) were used as purchased. Au substrates (300 nm epitaxial Au(111) layer on mica wafer, Georg Albert PVD, Heidelberg, Germany) were annealed using a natural gas flame before underpotential deposition of Ag or Cu was carried out.

UPD and SAM Formation. For Ag, Au/mica was immersed in 10 mM $AgNO_3$ in 100 mM HNO_3 (aq) and a potential of 10 mV (vs. Ag/Ag^+) was applied to the substrate for 2 minutes. This yields full coverage of a stable bilayer of silver atoms which follow the fcc stacking sequence of the underlying Au(111) substrate.[56-58] For Cu UPD, an incommensurate "(5×5)" Cu structure is formed by immersing Au/mica in 25 mM $CuSO_4$ + 5 mM KCl (aq) and applying a potential of 200 mV (vs. Cu/Cu^{2+}) for 1 minute.[59-61]

For SAM formation on Ag, the substrate was immersed in a 0.5 mM solution of surfactant molecule for 1 hour at 65°C. Since BPTCA is poorly soluble in pure water, a 1:1 mixture of H_2O and EtOH was used. After the immersions, the substrate was removed and thoroughly washed with EtOH before being dried using a flow of N_2 (g). On Cu, the substrate was immersed in 4mM BPTCA (aq) at 120°C for 1 hour in a sealed vial. The solution containing the substrate was then allowed to cool at room temperature for 15 minutes before the substrate was removed, thoroughly rinsed with EtOH and dried using a flow of N_2 (g).

Characterization.

Both samples were characterized at room temperature by scanning tunneling microscopy (STM) and by synchrotron based X-ray photoelectron spectroscopy (XPS) and near-edge X-ray absorption fine structure (NEXAFS) spectroscopy.

STM. STM imaging was carried out using a Molecular Imaging PicoSPM system in ambient atmosphere. Tips were cut from Pt/Ir 80:20 wire (Advent Research Materials Ltd., 0.25 mm diameter). Typical tunneling parameters of 0.5-0.7 V and 0.005-0.05 nA were used. To exclude irreversible changes between preparation in our lab and spectroscopic measurements under UHV conditions at the synchrotron, samples were characterized by STM before and after beam times.

XPS and NEXAFS. The measurements were performed at the bending magnet beamline D1011 at the MAX II storage ring of the MAX IV laboratory in Lund, Sweden. The XP spectra were collected using normal emission geometry at photon energies of 350 eV and 580 eV, depending on the binding energy (BE) range. The BE scale of every spectrum was individually calibrated using the Au $4f_{7/2}$ emission line of the Au substrate at 84.0 eV.[62] The energy resolution was better than 100 meV.

The XP spectra were fitted by symmetric Voigt functions using either a Shirley-type or a linear background, depending on the spectral range and primary photon energy. The fits were conducted self-consistently, using similar peak parameters for identical spectral regions.

The acquisition of the NEXAFS spectra was carried out at the C and O K-edges in the partial electron yield mode with retarding voltages of –150 and –350 V, respectively. Linear polarized light with a polarization factor of 95% was used. The energy resolution was better than 100 meV. The incidence angle of the light was varied from 90° (***E***-vector perpendicular to the surface) to 20° (***E***-vector near surface normal) to determine the orientational order in the BPTCA films. This approach is based on the dependence of the cross-section of the resonant photoexcitation process on the orientation of the electric field vector of the synchrotron light with respect to the molecular orbital of interest (so-called linear dichroism in X-ray absorption).[63]

Raw NEXAFS spectra were normalized to the incident photon flux by division through a spectrum of a clean, freshly sputtered gold sample. The photon energy (PE) scale was referenced to the pronounced π* resonance of highly oriented pyrolytic graphite at 285.38 eV.[64]

Calculations

To assist the interpretation of STM images, DFT calculations of the isolated molecules were performed using Gaussian 98W.[65] After energy minimization using B3LYP/G6-31+(d,p) which yields a structure with a twist angle between the two phenyl rings of about 40°. For the orbital calculations the twist angle was adjusted to 20°. The choice of this geometry was motivated by the arrangement of the molecules in the layers such that the dimensions of the different H-bonds between carboxylic acids groups were in the same range.

RESULTS AND DISCUSSION

STM

BPTCA on UPD-Ag: Adsorption of the molecule on silver at room temperature or slightly elevated temperatures yields layers as presented in Figure 1. The large scale image (Figure 1a) shows a highly structured surface with, however, no obvious long range order. Higher magnification (Figure 1b) reveals that short striped features appearing bright coexist with darker, usually featureless patches. This morphology is not significantly dependent on the adsorption time which was varied between a minute and one hour. Analyzing high resolution images such as the ones shown in Figures 1c and 1d, three levels of tunneling contrast are observed. Mainly, protrusions arranged in straight or bent rows are seen with an intrarow separation of about 3.5-4 Å and an interrow distance of 9-10 Å. These are mixed with isolated protrusions appearing higher by 1-1.5 Å and small patches appearing lower by 3-4 Å, respectively. The short intrarow distance of the protrusions implies that the rows consist of upright standing molecules. While it was difficult to observe any features in the dark patches, a row structure could be resolved in cases where the patches are sufficiently large (see inset of Figure 4d), even though we were not able to clearly identify an intrarow structure. Based on the substantial height difference between the rows we suggest that the features in the patches arise from flat lying molecules.

A closer look at high resolution images such as Figure 1c reveals different arrangements of the molecules, which are described by a rectangular and oblique unit cell, respectively. The former arises from the in phase arrangement of the molecules in adjacent rows (marked by dashed white lines) and is the dominating structure for samples prepared at room temperature. The latter represents the smaller fraction and is defined by a shift between neighboring rows as highlighted by the solid white lines in Figure 1c.

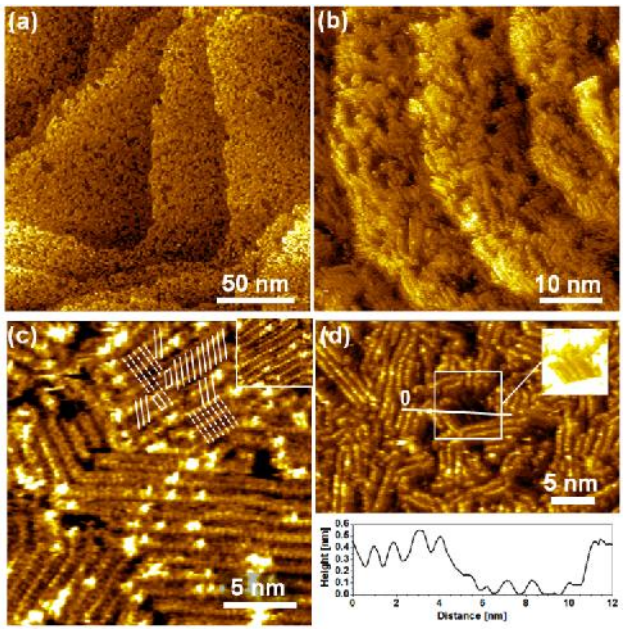

Figure 1. STM images of BPTCA adsorbed on UPD-(1×1)Ag/Au from a 0.5 mM solution in 1:1 EtOH/H_2O for 10 min at 293 K (a,b) and 1h at 293 K (c) and 306 K (d). White dashed and solid lines in c) highlight the coexistence of different alignments and unit cells. Inset shows unobstructed view of this area. Inset in d) shows the framed area at different contrast.

Since, as mentioned, longer immersion times did not significantly improve the layer quality, preparation at elevated temperatures was investigated. It is seen from Figure 2a that, even though regions with straight and bent rows still coexist, the areas of parallel rows are now more abundant and significantly more extended compared to the samples prepared at room temperature. Also, the number and size of the dark patches are strongly reduced. Similar to the samples prepared at room temperature, bright protrusions are observed, which are precisely in line with the rows as evidenced by the high resolution image of Figure 2b. We exclude that they originate from contamination since their occurrence and concentration does not depend on whether BPTCA is used as purchased or recrystallized before use. The intra- and interrow distances amount to 3.5-4 Å and 9-10 Å, respectively, as inferred from the corresponding height profiles depicted in Figure 2b. While these are the same dimensions as

observed for the room temperature sample there is a decisive difference between them. For the sample prepared at elevated temperature only the oblique unit cell is observed in areas where rows are well aligned. This structure exhibits two characteristic features which are revealed in high resolution images such as the one seen in Figure 3a. The first feature is the occurrence of streaks between two protrusions orientated at an angle of about 55°, approximately along the long side of the unit cell shown. The other one is the elongated shape of the protrusion with the long axis aligned with the direction of the height profile B, i.e., rotated about 55°-60° vs. the molecular rows. We note at this point that the tunneling contrast can significantly vary due to tip changes as highlighted by the inset in the image of Figure 3a in which these features are barely seen. They are, however, not imaging artifacts due to particular tip geometry as proven by scanning with a rotated scan direction and by their appearance in differently orientated domains. They will be addressed in more detail below when discussing structural models.

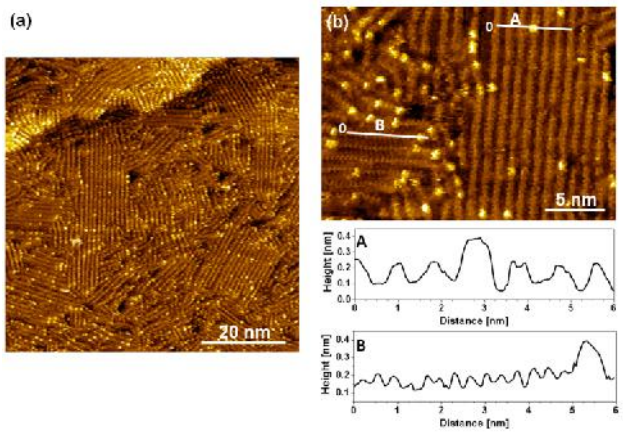

Figure 2. STM images of BPTCA on UPD-(1×1)Ag/Au prepared at 338 K and 1h immersion time. Height profiles along lines A and B in the high resolution image (b) are shown in (c).

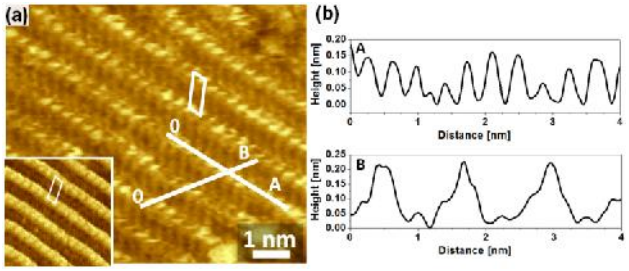

Figure 3. High resolution STM image of BPTCA on UPD-(1×1)Ag/Au prepared at 338 K with oblique unit cell indicated. Inset demonstrates variation in tunneling contrast for the same sample. b) Height profiles along (A) and intersecting (B) molecular rows.

BPTCA on UPD-Cu: In contrast to TMA for which SAMs on Ag and Cu modified Au substrates could be formed under identical conditions, the formation of BPTCA layers on copper turned out to require preparation parameters very different from those applied for the Ag substrates. Preparation from an EtOH/H_2O solution at room temperature produced images like the one depicted in Figure 4a with, at best, some small isolated patches where a row structure is discernible. Since variation of the parameters, i.e., temperature, concentration and the EtOH/H_2O ratio did not improve the results, preparation from pure water was attempted. At room and elevated temperatures images like Figure 4b were obtained, which lack any row structure but, instead, showed Y-shaped features which are randomly oriented and can be assumed to represent flat lying molecules. Since for TMA such a flat lying structure has not been observed[41-43] we suspected that the additional benzene ring of BPTCA might shift the equilibrium from the tilted geometry observed for TMA towards the flat lying phase due to the additional interaction of the second aromatic ring with the substrate. Indeed, upon a further significant increase in the preparation temperature, islands exhibiting the row structure familiar from TMA started to form and, within a rather narrow temperature range of about 10°C, a pronounced improvement in the film structure was observed, as evident from

the comparison of Figures 4c and 4d. However, even at 120°C the fraction of the areas showing darker contrast remained significant and, notably, increased again for temperatures beyond this value. The homogeneity of the layer was successfully improved by increasing the concentration of BPTCA. Using a 4 mM solution, uniform SAMs such as the one shown in Figure 5 were obtained with well-defined domains of BPTCA, typically about 400-500 nm^2 in size. In contrast to the structure found on the Ag UPD layer, the rows on the pseudomorphic Cu-UPD layer are well aligned with the $<11\bar{2}>$ directions of the Au substrate. A quantitative analysis of the intrarow distances yields 5.2±0.3 Å and the average value for the interrow distance is 9.0±0.3 Å, which suggest that the molecule forms a SAM isostructural to the one reported for TMA on Cu-UPD/Au(111).[41-43]

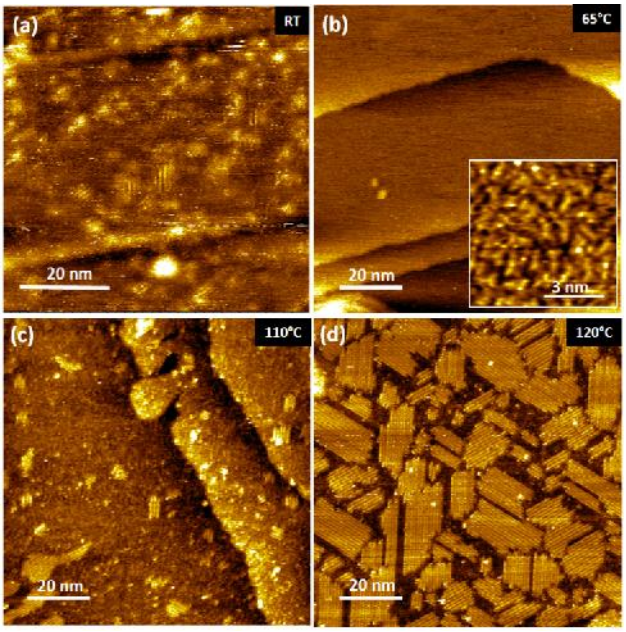

Figure 4. STM images of BPTCA on UPD-(√3×√3)Cu/Au prepared under different conditions. a) 1 mM solution in 1:1 EtOH/H2O, 1h at room temperature. b-d) 2 mM solution in pure H2O, 1h at temperatures as indicated in the images.

A number of points are noteworthy here, which will be crucial in the discussion of the structural models below. Firstly, with adjacent rows shifted against each other as seen from

the high resolution image in Figure 5c, the structure is described by a rectangular 6×√3 unit cell containing two molecules. Secondly, unlike TMA where the interrow distance can adopt three different values, all rows are equally spaced by three Au-Au distances. Thirdly, the structure of the BPTCA SAM is independent of the details of the UPD layer, which can be prepared with different packing of the Cu atoms and adsorbed anions.[59, 66-67] A chloride terminated (5×5) Cu-UPD structure yields the same results as BPTCA and trimesic acid on a sulfate terminated (1×1) and (√3×√3) Cu-UPD substrate.[41-42]

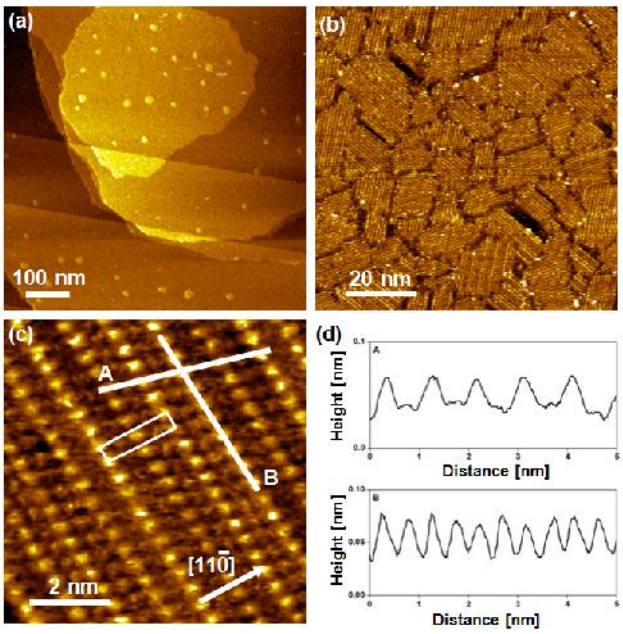

Figure 5. a-c) STM images at different magnifications showing the monolayer of BPTCA on UPD-(5×5)Cu/Au surface prepared from a 4 mM aqueous solution at 120° C for 1h. The 6×√3 unit cell is indicated in c). Height profiles along lines A and B marked on image (c) are shown in (d).

XPS

Since the differences between the Ag and Cu modified gold substrates observed in the STM images resemble those of TMA[41-42] samples of the quality shown in Figures 2 and 5 were

analyzed by XPS in order to elucidate the bonding configurations. The C 1s spectra (Figure 6) contain emissions characteristic of free COOH (~288 eV) and COO^- groups (~287 eV). The signal of the aromatic rings appears at 284.1-284.5 eV together with a small additional peak shifted to higher binding energies. This spectral feature at binding energies higher than the main peak has also been observed in other types of biphenyl based SAMs[68-71] and is interpreted to arise from chemically shifted carbon bonded to electronegative atoms such as sulfur or oxygen, and/or shake-up transitions.[72] For BPTCA we favor the latter as no chemical shift of the ring carbon is expected. For the purpose of analysis, all spectra were fitted with these four components. For a consistent set of fits the peak width and positions were fixed for all but the large signal and the results are compiled in Table 1. It is noted that for the Ag substrate a satisfying fit of the carboxylic acid signal requires a larger peak width than for Cu, which is interpreted to result from the different environments of the COOH moieties in the respective SAMs, as discussed in more detail below.

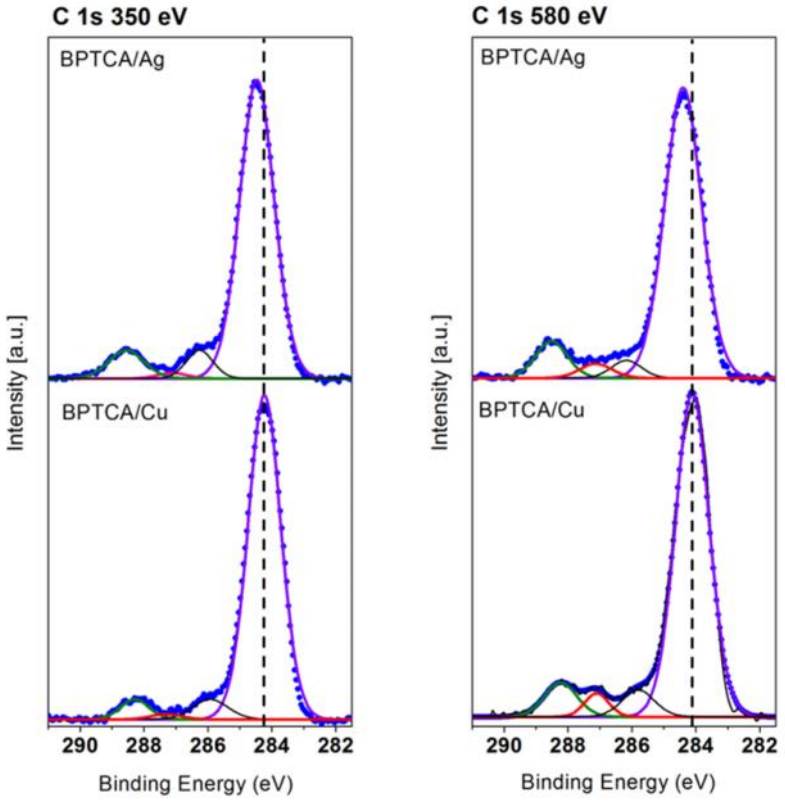

Figure 6. C 1s XP spectra of BPTCA on UPD-Cu (bottom) and UPD-Ag (top) acquired at photon energies of 350 eV and 580 eV. Components for the aromatic backbone (violet and black), the COO^- (red) and COOH (green) have been fitted.

Table 1. Intensity ratios, binding energies (BE) and peak widths (fwhm) from the C 1s XP spectra of BPTCA on Cu and Ag UPD substrates at photon energies of 350 eV and 580 eV.

	C_{COOH}/C_{COO-}		$C_{biphenyl}/(C_{COO-})$	
	Ratio	BE (fwhm) [eV]	Ratio	BE (fwhm) [eV]
Ag UPD				
350 eV	4.7	288.50 (1.3) 287.10 (1.0)	53.0	286.20 (1.0) 284.46 (1.28)
580 eV	2.8	288.50 (1.3) 287.10 (1.0)	20.1	286.14 (1.0) 284.40 (1.37)
Cu UPD				
350 eV	3.6	288.26 (1.0) 287.08 (1.0)	67.3	286.98 (1.0) 284.24 (1.21)
580 eV	1.2	288.26 (1.0) 287.08 (1.0)	15.5	285.86 (1.0) 284.12 (1.27)

For the main emission associated with the biphenyl unit, a small substrate dependent shift of ~0.25 eV is observed, giving a slightly higher binding energy for this component on Ag. This effect, which is also observed for trimesic acid on Ag and Cu modified gold substrates,[41] can be explained by the differences in the packing densities of each monolayer, as revealed by the STM images. Essentially, the same difference is observed for the free COOH group whereas, interestingly, there is no indication of a substrate dependent shift of the carboxylate signal.

Looking at the intensity ratios of the individual emissions one finds a clear dependence on the photon energy. For the photon energies used the escape depth of the C 1s photoelectrons is rather small and varies significantly with photon energy, thus, resulting, on the one hand, in a pronounced deviation of the C 1s signal from the stoichiometric values but, on the other hand, in providing qualitative structural information. Due to the small carboxylate signals, the precision of the values given is limited. However the intensity ratios, nevertheless, reveal certain trends. In particular, on both substrates the $COOH/COO^-$ ratio is significantly lower for a photon energy of 580 eV compared to 350 eV. Since the photoelectron signal is less attenuated at higher kinetic energy of the photoelectrons, the change in the ratio is consistent

with the carboxylate being buried at the SAM-substrate interface and the COOH forming the outer surface of the monolayer. Notably, the change of the ratio with photon energy is smaller on Ag than on Cu, which supports the interpretation that, in analogy to trimesic acid[41], BPTCA forms SAMs with a bipodal and monopodal adsorption geometry on Cu and Ag, respectively. With only one carboxylate binding to the substrate in the case of Ag, the change is expected for stoichiometric reasons to be less than on Cu with two carboxylates per molecule.

The principal difference in the adsorption geometries of BPTCA on Cu and Ag becomes even clearer when looking at the O 1s XP spectra shown in Figure 7. The experimental data are well described by three components representing the carboxylate (~530.7 eV), carbonyl (~531.5 eV) and hydroxyl (~532.9 eV) oxygens.[23, 41, 73] In fitting these components, the hydroxyl and carbonyl oxygens of the free carboxylic acid groups have been set to the stoichiometric ratio of 1:1 and the COO^- signal was fixed in position and width to 530.7 eV and 1.1 eV, respectively. The results are compiled in Table 2. Similar to the C 1s signal, the emissions related to the free COOH exhibit substrate dependent peak widths which, once more, reflect structural differences in the films. We note that on Cu a reasonable fit (even though a good than the one shown in Figure 7) can also achieved with an equal width of both peaks but on Ag different values are required. This is in line with the similar behaviour of the C1s signal of the COOH moiety discussed above and further corroborates that the environment of the COOH group is less homogeneous on Ag than on Cu (*vide infr*a). Another obvious difference is the pronouncedly higher intensity of the carboxylate peak for BPTCA on Cu compared to Ag, which is further evidence of the bipodal bidentate anchoring on the copper UPD surface compared with a monopodal bidentate geometry on Ag.

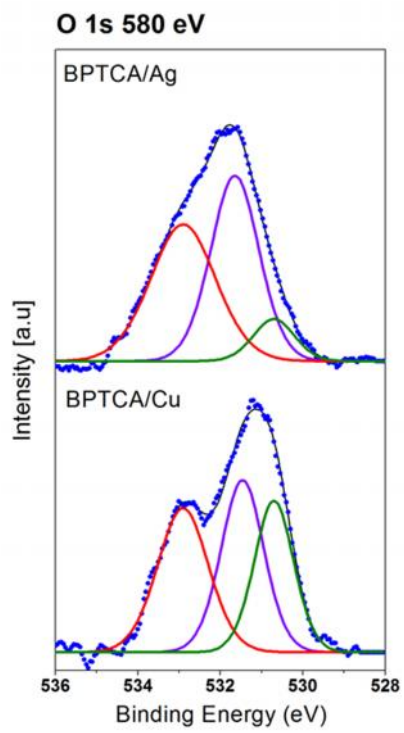

Figure 7. O 1s XP spectra for BPTCA on UPD-Ag (top) and on UPD-Cu (bottom) taken at a photon energy of 580 eV. Components assigned to the carboxylate (green), carbonyl (violet) and hydroxyl (red) oxygen atoms have been fitted.

Table 2. Intensities, peak widths (fwhm) and binding energies (BE) from the O 1s XP spectra of BPTCA on Cu and Ag UPD substrates at a photon energy of 580 eV.

		COO^-	C=O	C-OH
Ag	Intensity [rel. u.]	0.21	1.0	1.0
	FWHM [eV]	1.10	1.3	1.80
	BE [eV]	530.70	531.66	532.92
Cu	Intensity [rel. u.]	0.77	1.0	1.0
	FWHM [eV]	1.10	1.21	1.45
	BE [eV]	530.70	531.46	532.90

Assuming upright standing molecules and neglecting differences in molecular tilt and packing density, a simple calculation lends additional support of the structural differences.

For the monopodal geometry on Ag, a value of 2 is expected for the COOH/COO^- oxygen ratio. Assuming that the COOH is located at the outer SAM surface and, thus, its signal is not attenuated, the observed significantly larger ratio of 2/0.21 = 9.5 arises from the attenuation by a factor of 4.8 of the photoelectrons from the carboxylate moieties buried at the SAM-substrate interface. In contrast, on Cu with two carboxylate moieties and one COOH group at the buried and outer interface, respectively, the stoichiometric COOH/COO- ratio is 0.5. The observed value of 2/0.77 = 2.6 yields an attenuation factor of 5.2 which, considering the crudeness of the model, is considered to be in a good agreement with the above value. It is noted that in the case of BPTCA the intensity ratio of the carboxylate oxygen and the C-OH/C=O signals is significantly smaller compared to the analogue TMA[41] because of the stronger attenuation of the carboxylate signal from the buried SAM-substrate interface by the additional benzene ring. In summary, the XPS data corroborate the analogy between TMA[41-42] and BPTCA with respect to the substrate dependent bonding configuration.

NEXAFS

The C and O K-edge NEXAFS spectra of BPTCA on both copper and silver are compiled in Figure 8. The spectra acquired at an X-ray incident angle of 55° ("magic angle") are shown on the left and the 90° - 20° difference spectra are given on the right. The "magic angle" spectra probe the unoccupied orbitals of the molecules in the SAMs without any contributions arising from the effects of the orientation of the molecules. These effects are revealed by examining the differences in the spectra acquired at X-ray incident angles of 90° and 20°. The presence of molecular orientation in the system being studied is then exhibited by the occurrence of pronounced difference peaks at the positions of the absorption resonances. This is indeed the case for the BPTCA films on both Ag and Cu, indicating a high orientational order in these monolayers.

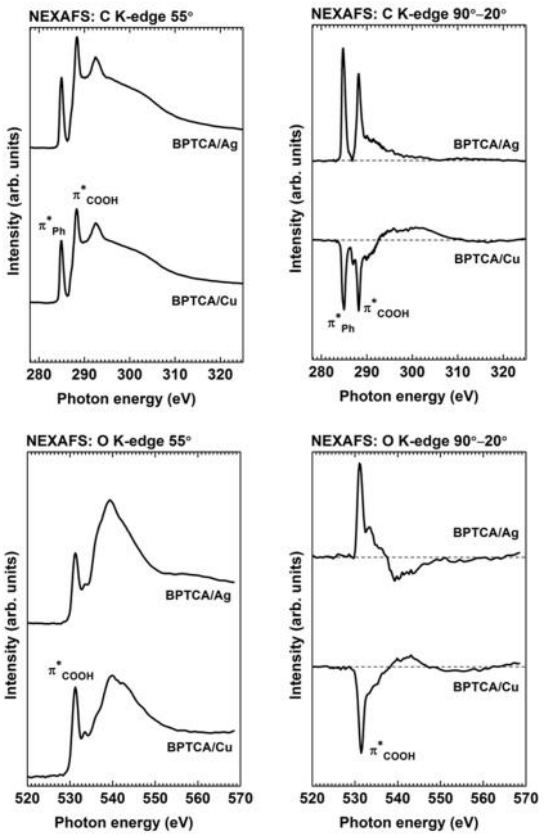

Figure 8. NEXAFS spectra of BPTCA on UPD-Ag and UPD-Cu modified Au(111)/mica surfaces. The most pronounced absorption resonances are assigned. Left panels: Spectra recorded at an angle of X-ray incidence of 55° with respect to the surface plane. Right panels: difference of the spectra recorded at 90° (normal incidence) and 20° (grazing incidence).

The main resonances dominating the 55° C K-edge spectra on both copper and silver modified surfaces can be assigned to transitions into the unoccupied π^* orbitals of the biphenyl system (~285 eV) and the carboxylate/carboxylic acid groups (~288 eV) of BPTCA.[63, 74] In the O K-edge spectra, the sharp pre-edge resonance can be assigned to transitions into the π^* orbital of the carboxylate/carboxylic acid groups (~531 eV). It is noted that the resonances associated with COOH moieties comprises contributions from both COOH and COO^-. Furthermore, since more than one moiety of both the carboxylic acid

groups and the aromatic rings contribute to the respective signals, the experiment yields an average value. However, due to the attenuation of the electrons, which is weaker than in the XPS case but still considerable,[75] the individual moieties might contribute to a varying extent, depending on their locations within the layer.

Both C K-edge and O K-edge 55° spectra of BPTCA show no significant differences on Cu as compared to Ag. In contrast, the 90°-20° difference spectra for these two substrates are distinctly different. Indeed, the peaks for the SAM on silver appear with a positive intensity, while on copper it is negative. This pinpoints a substantial substrate dependence of the molecular orientation.

The quantitative evaluation of the entire set of the NEXAFS spectra gives the average orientation of the transition dipole moments (TDMs) of the most relevant molecular orbitals. The resulting values, compiled in Table 3, suggest significant differences in the orientation of the TDMs for the two substrates, whereas the differences between the TDMs of the aromatic rings and the carboxylic acid moieties for each system are minor. Interestingly, for the COOH/COO^- groups the values from the C and O K-edges are essentially identical on Ag whereas they diverge slightly more on Cu. However, for the latter the difference is about half as big as reported for TMA.

The correlation of the TDMs with the molecular orientation is, in general, not trivial. Even though the directions of the TDMs are well defined by the respective functional units (perpendicular to these units due to the π^* character of the molecular orbitals involved), it is not straightforward because of the conformational degrees of freedom of the molecule described by various twist angles ϑ_n, which are defined in Figure 9a. On Ag where a monopodal adsorption geometry is realized, the similarity of the orientation of the TDMs of the carboxylic acid groups and the aromatic rings indicates that the molecules are adsorbed in an essentially coplanar conformation. With a tilt angle of the TDMs of about 60-65° from the

surface normal this seems at first glance homologous to TMA[41] and would be described by the symmetric configuration shown in Figure 9b. However, for BPTCA there is another possible monopodal adsorption geometry, which is the asymmetric configuration depicted in Figure 9c and which, as discussed in detail below, is thought to be realized. In either case, the molecule stands rather upright with the tilt angle φ amounting to 25-30°.

On Cu the TDMs are orientated more towards the surface normal, i.e., the molecules are more tilted compared to Ag. Contrasting the monopodal geometry on Ag where, in principle, a bidentate binding can be realized for BPTCA if the COOH/COO^- moieties are coplanar with the aromatic ring, interpreting the similarity of the ring and COOH/COO^- tilt angles in terms of coplanarity is incompatible with the bipodal/bidentate geometry on Cu. For this system the carboxylate groups have to rotate out of the ring plane as illustrated in Figure 9a, yielding significantly different values of the tilt angle for the respective TDMs. Several possibilities can explain this discrepancy, one of which is that the signal from the buried carboxylate groups is significantly attenuated and, thus, the dominating contribution comes from the top COOH group which, it is reasonable to assume, is coplanar with the aromatic ring. Further possibilities are that due to the interaction of the COO^- groups with the substrate, the simple picture of the TDM being orientated orthogonal to the O–C–O plane is inappropriate or that the interface is restructured to an extent that the oxygen atoms are not in the same plane. Studies of biphenyl-3,5-dicarboxylic acid, the BPTCA analogue without the COOH group in the 4-position, should be able to shed some light on this point.

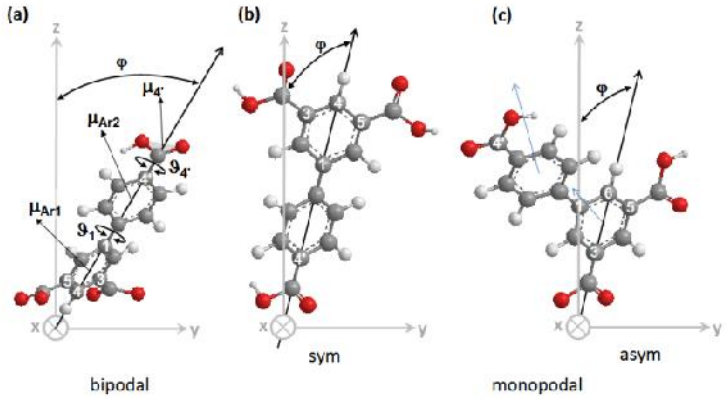

Figure 9. Illustration of adsorption geometries for BPTCA. (a) bipodal and (b,c) monopodal configurations. The tilt angle φ of the molecule is defined by axes through the respective C-atoms and the surface normal z. Twist angles ϑ_n define rotations around bonds of the respective C-atoms. Coplanarity of the aromatic rings and the planes of the COOH/COO^- moieties is defined by $\vartheta_n = 0°$. For clarity the twist angle of only one carboxylic acid group is indicated in (a). The directions of the TDMs (μ) associated with the different structural units are shown in (a).

Table 3. NEXAFS derived orientation of transition dipole moments of the π* orbitals of the phenyl rings and carboxylic groups for the BPTCA SAMs on Cu and Ag modified Au/mica. Values are vs. the surface normal.

	Tilt angle ρ [°]		
Sample	Ring (C K-edge)	COOH/COO- (C K-edge)	COOH/COO- (O K-edge)
On Cu UPD	49.3	48.8	43.6
On Ag UPD	64.7	60.2	61.7

Structural Models

BPTCA on Cu: The commensurate row structure with rows aligned along the <11$\bar{2}$> direction of the substrate (see Figure 5) is characteristic of the bipodal adsorption geometry of isophthalic acid. Obviously, the additional phenyl ring in BPTCA does not result in a fundamental change of the layer structure compared to the smaller analogues such as IPA or TMA[42] and thus confirms that due to the strong Cu-carboxylate bond the substrate lattice plays a decisive role for the molecular packing. The bipodal adsorption of the molecules and their arrangement in a 6×√3 unit cell results in a density of the carboxylate head groups of 4.6×10^{14} cm^{-2} which, incidentally, is the same widely observed for the sulfur head group in thiol SAMs.[76-77] In this context it is noted that an adsorption geometry where the molecules bind in a bipodal geometry through the carboxylic acids groups in 3 and 4' position can be excluded. It would be sterically more demanding and, thus, would result in a larger interrow distance than observed. Furthermore it yieldw a lower density of the carboxylate groups compared to the IPA configuration which is enthalpically unfavourable.

While the IPA/TMA and BPTCA layers exhibit the same interrow separation and distance of the molecules along the rows, the different size of the molecules, nevertheless, gives rise to differences at a more detailed level. Characterized by a 6×√3 unit cell, BPTCA follows a regular pattern due to a shift of half the intermolecular distance between adjacent rows and a single value for the interrow spacing (8.67 Å) as evidenced by the high resolution image of Figure 5c. In contrast, a 9×√3 unit cell for IPA and a less regular repeat pattern for TMA are observed, with three different values (a = 8.2 Å, b = 8.8 Å, c = 9.05 Å, see Figure 10) of the interrow spacing. These features were explained by a rotation of the 1,4-axis out of the (11$\bar{2}$) mirror plane and the occurrence of opposite tilt directions as illustrated in the bottom part of Figure 10.

For the sterically more demanding BPTCA molecule, the configuration with an antiparallel arrangement of the molecules and tilt towards each other (rows 1-2 in the IPA model) is

sterically not possible. Only the configurations where the molecules are arranged in parallel (rows 2-3) or antiparallel but pointing away from each other (rows 3-1) can be realized, with the latter being only possible at domain boundaries. However, assuming identical adsorption sites in the parallel configuration, adjacent molecular rows are in phase, which would mean a $3\times\sqrt{3}$ unit cell that is in conflict with the out of phase arrangement seen in the STM images. Matching the experimentally observed unit cell by shifting every second row of the molecules by half a unit cell length along the $<11\bar{2}>$ direction yields the model shown in the top part of Figure 10. At this point we note two things which are related. The first one is that we have no experimental knowledge of the exact adsorption sites of the oxygen atoms of the carboxylic acid groups. Contrasting models from upright standing simple monocarboxylic acids on Cu where the oxygens are positioned on top sites,[78] the molecules have been positioned with oxygens essentially located in bridge sites. This is based on DFT calculations on IPA based SAMs which will be discussed in a forthcoming publication. The second point is the rotation of the molecules out of the $<11\bar{2}>$ mirror plane which is based on the IPA model. A symmetric arrangement with the 4,4'-axis in the mirror plane is also conceivable. However, we favor the rotated geometry at this point as this matches the high resolution STM images such as the one of Figure 5c, which shows structural features orientated at an angle of about 75° rather than 90° relative to the row axis.

The last point we would like to address for the BPTCA monolayer on Cu-UPD is the question of the striking difference in the preparation conditions compared to IPA/TMA SAMs which form easily at room temperature. Considering the lack of knowledge about the SAM-substrate interface, we stress the speculative nature of our reasoning. The high temperature required strongly suggests that a significant activation barrier has to be overcome in order to form an ordered layer. To be incorporated into a domain, the sterically more demanding BPTCA molecule is likely to impose more stringent conditions on the diffusion of

the two coupled carboxylic acid groups compared to IPA/TMA. The reduction to less favorable pathways and/or the generation of kinetic traps would have to be compensated by a higher temperature. While the higher temperature facilitates formation of ordered domains it shifts the chemical potentials towards the solution phase by increasing the solubility of the substance. This effect might even take over at one point, thus, decreasing again the film quality, which is indeed observed in our experiments. This argument is also supported by the fact that an increase in concentration significantly improves the quality of the layer as evidenced by Figures 4d and 5b. The surprisingly narrow temperature range for the formation of the BPTCA layer is, therefore, the result of a superposition of a kinetic and a thermodynamic effect.

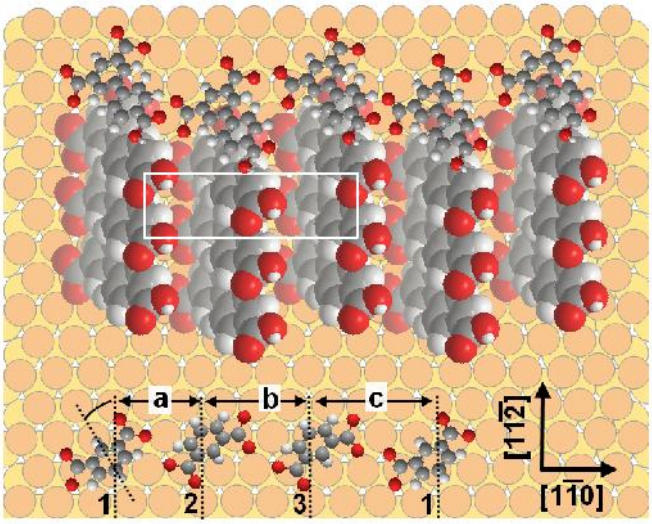

Figure 10. Structural model of BPTCA monolayer on UPD-(1x1)Cu/Au(111) surface with $6\times\sqrt{3}$ unit cell marked by white rectangle. For comparison the model proposed for IPA[43] is shown at the bottom. For details see text.

BPTCA on Ag: In contrast to Cu where the strong molecule-substrate interaction results in the formation of a commensurate layer, the structure of the BPTCA layer on Ag is dominated by

intermolecular interactions. The significantly weaker molecule-substrate bond makes it more favorable for BPTCA to maximize intermolecular interactions, which is reflected by the fact that the molecule adopts a monopodal adsorption geometry. This results in a density of the carboxylate moieties which, for the crystalline structure obtained at elevated temperature (Figures 2 and 3), amounts to about 2.8×10^{14} cm^{-2} (9.5 Å × 3.8 Å = 36$Å^2$) and is significantly lower compared to the 4.6×10^{14} cm^{-2} found for the bipodal binding on Cu. Note, however, that the packing density of the molecules is higher on Ag than on Cu (43.2 $Å^2$) since there is one adsorbed molecule for every carboxylate anchor in the former case, in contrast to one molecule per two carboxylate anchor groups in the latter case.

The two free carboxylic acid moieties of the BPTCA molecule enable intermolecular interactions through hydrogen bonding. Similar to TMA studied previously,[41] this represents a substantial enthalpic contribution, which adds to the one arising from the interactions between the aromatic rings. The crucial influence of the H-bonding is also in accordance with the fact that, unlike on UPD-Cu, the structure is not as well defined on a large scale with bends in the rows and variations in the interrow distance frequently occurring (see Figure 1). As known from bulk crystal structures there is a considerable variability in the geometries involving H-bonding in aromatic carboxylic acids,[79] which is consistent with the interpretation that the energy hypersurface of the BPTCA layer contains a manifold of local minima.

Compared to TMA, BPTCA has additional degrees of freedom which are the torsion angle ϑ_1 of the two phenyl rings (see Figure 9) and, due to the lower symmetry of the molecule, two distinctly different possibilities for the adsorption geometry, denoted as sym and asym (see Figure 9b,c). For the more symmetric configuration (Figure 9b) which is the one analogous to TMA, the 4-4' axis defines the molecular tilt. For the asymmetric adsorption geometry (Figure 9c) the tilt angle is defined by the 3-6 axis.

For the discussion of possible configurations we refer to Figure 11a, which displays different arrangements and conformations of the molecules and schematic representations of the corresponding unit cells. Structure **i** where the molecules adopt the sym configuration is analogous to the one observed for TMA. This arrangement is described by a rectangular unit cell (**1** in Figure 11a) and is consistent with one of the structures found for layers prepared at low temperature (see Figure 1c). For this arrangement where the phenyl rings are coplanar, the distances between the nearest oxygen atoms of adjacent molecules are about 2.5 Å, i.e., well in the range of values reported for hydrogen bonding in aromatic carboxylic acids. A shift between rows as also observed in Figure 1c would produce the oblique unit cell **2** and a larger O-H···O distance compared to structure **1**. Notably, from the structural features seen between the rows of protrusions, there seems to be some alignment along the unit cell axis, which links next nearest neighbors in adjacent rows rather than nearest neighbors. Thus, unit cell **4** looks like a better description than **3**. Such an alignment can be easily realized considering the possibility that the phenyl rings in BPTCA might be rotated against each other as shown in model **ii** of Figure 11a. Another possibility to generate such an alignment is a coplanar geometry but a tilt of the 4-4' axis of the molecule in a direction not along the molecular rows as shown in model **iii**. It is noted that in model **ii** the carboxylic acid groups of the molecule are at different heights whereas in model **iii** they are at the same height. Irrespective of the exact positions of the carboxylic acid groups, for both geometries the O–H···O distances are above 4 Å, which would mean a significantly reduced H-bonding and, thus, questions the thermodynamic stability of this structure compared to the one with the rectangular unit cell.

While the resolution in the samples prepared at lower temperatures is not sufficient to draw any more detailed conclusions, the samples prepared at elevated temperature reveal additional structural features as seen from the comparison of Figures 1c with 2b and 3. These are

pinpointed by the image displayed in Figure 11b, which shows the drift corrected, unit cell averaged STM image of Figure 3. The image highlights the characteristic zig-zag pattern which consists of elongated and asymmetric protrusions aligned along *a* and parallel line type features of lower contrast running along *b*. The latter alternates with elliptically shaped areas of even lower contrast. The two directions are orientated at angles of 30° and 145° relative to the y-axis.

In order to correlate the STM image with the film structure, we make the reasonable assumption that at the rather low tunneling currents used in this study the outer surface of the layer is imaged.[80] Since at the bias applied tunneling is non-resonant, a further simplifying assumption is made, which is that the lowest unoccupied molecular orbital (LUMO) dominates the tunneling.[81-82] It is noted that the molecular orbitals are based on calculations of the isolated neutral BPTCA molecule, i.e., no bonding to the substrate is taken into account. The rationale behind this is that for upright standing molecules the MOs of the molecule should not be fundamentally affected by the comparably weak BPTCA-Ag coupling.

For the sym configuration, the structural model and the LUMO are shown in the top right corner of Figure 11b. The molecular fragments have been positioned such that the biggest and outermost lobe of the LUMO, which is the π orbital located at carbon atom 4, matches the bright protrusion. For the azimuthal alignment the ring plane is orientated parallel to the direction *a*. As can be seen, there is only partial agreement between the model and the experiment. In particular, the model does not well reproduce the pattern of the dark ellipses and lines connecting the molecular rows. This, in addition to the large O–H···O distances mentioned above, motivated the consideration of the asym configuration as defined in Figure 9c.

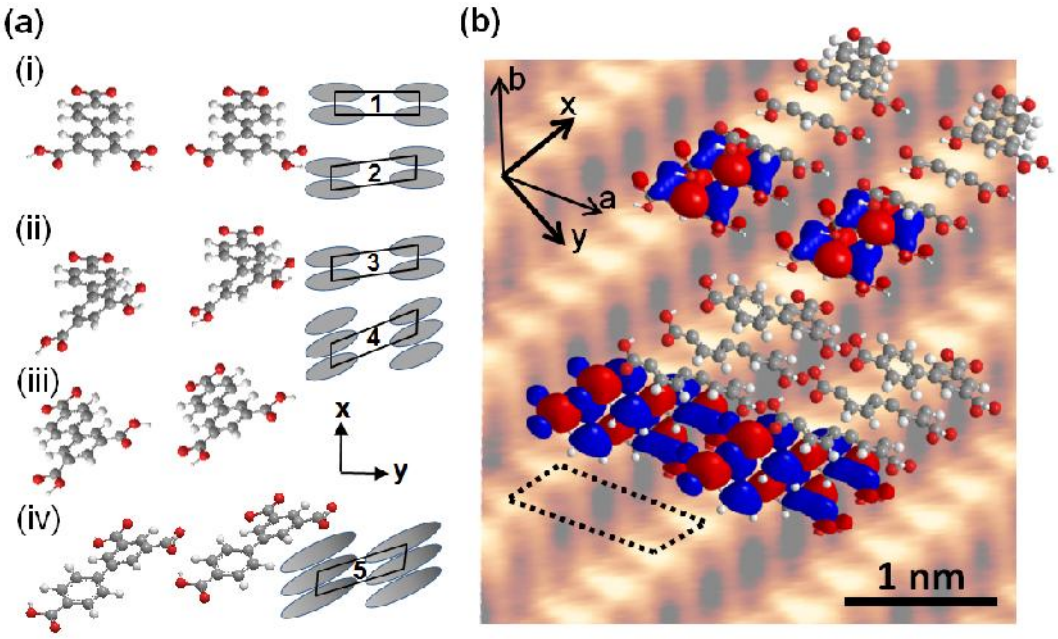

Figure 11. Models of the BPTCA monolayer on UPD-Ag. (a) Different configurations comprising sym (i-iii) and asym (iv) arrangements together with possible unit cells. (b) Molecular structures including LUMO overlaid on unit cell averaged STM image. Shown are models iii (top) and iv (bottom). Dotted line indicates unit cell. For clarity only the topmost atoms are shown for some of the molecules and the part of the LUMOs below the atomic plane has been omitted. For details see text.

In this case there is no gap between the molecular rows and the O–H···O distances, which are in the range of 2.2-2.4 Å and match the dimension typical for H-bonding in carboxylic acids. It is worth noting that the exact value depends on how much the second aromatic ring is rotated against the IPA ring. The course of the LUMO in this asymmetric arrangement matches the image significantly better than the symmetric configuration. Since the asym configuration is in perfect agreement with the dimensions of hydrogen bonding and is in good agreement with the tunneling contrast we suggest that this is the geometry realized for the BPTCA. We finally note two points. Firstly, the asym configuration involves a complex

interaction between the COOH groups whereas on Cu the free COOH group is rather isolated which is consistent with the observed that in the fits of the C-OH and C=O peaks (Figure 7, Table 2) substantially different fwhm values are required for Ag but not for Cu. Secondly, this geometry could also explain the bright protrusions observed (e.g. see Figure 2b) if it is assumed that these are molecules trapped in a sym configuration. Figures 9b and 9c illustrate that the sym arrangement extends further than the asym one.

CONCLUSIONS

The present study of BPTCA consolidates the pronounced substrate dependence of the monolayer assembly of aromatic carboxylic acids first observed for trimesic acid[41] and the isophthalic acid moiety as a base unit on UPD-Cu substrates.[42] The bipodal adsorption geometry reflects the fact that the dominating contribution to the enthalpy of formation of the SAM comes from the molecular-substrate interaction. Therefore, the major force driving the self-assembly is the maximization of the density of carboxylate-metal coordination bonds. The symmetry of the isophthalic acid moiety enforces a characteristic row structure where the intrarow and interrow distances are determined by the periodicity of the molecule-substrate corrugation potential and the footprint of the isophthalic acid moiety. Thus defining the molecular packing this also determines to what extent the carboxylate groups are forced into an energetically unfavorable conformation out of plane of the aromatic ring, which is required to realize the bidentate coordination geometry.

Depending on the substitution in the 5-position of the isophthalic acid moiety, additional factors play a role which affect both the kinetics of film formation and details of the row structure. Steric requirements account for the latter whereas the former is reflected in a striking difference in the preparation temperature of TMA and BPTCA SAMs. Furthermore,

a surprisingly narrow temperature window exists for the BPTCA SAM to form which we believe arises from a combination of kinetic and thermodynamic factors.

The UPD-Ag substrate, where the intermolecular interactions dominate over the molecule substrate interactions offers, on the one hand, the opportunity of flexibility in the design of SAMs of coordination bonded molecules. On the other hand, for these 2D systems one is faced with polymorphism analogous to bulk supramolecular structures. This is illustrated by the example of BPTCA which, depending on the preparation conditions, can exhibit different and/or coexisting adsorption geometries. As BPTCA illustrates, a systematic variation of the SAM structure through changes of the molecular architecture might be less straightforward to predict on Ag compared to Cu, unless the molecule exhibits a highly symmetric structure.

The bipodal adsorption geometry on UPD-Cu and the monopodal one on UPD-Ag, i.e., the substrate dependent preference of the isophthalic acid or benzoic acid binding motif, realized for both BPTCA and TMA SAMs raises the question of how oligophenylene monocarboxylic acids behave. While on UPD-Ag a dense packing of upright standing molecules can be expected, the situation is not clear for the UPD-Cu surface. Current studies are aimed at elucidating the behavior of this class of molecules.

ACKNOWLEDGMENTS

Support by The Leverhulme Trust and an EPSRC doctoral training grant is gratefully acknowledged. We thank the staff of the Max IV laboratory, and A. Preobrajenski in particular, for the technical support during the synchrotron-based experiments. This work was supported by funding from the European Community's Seventh Framework Programme (FP7/2007-2013) CALIPSO under grant agreement nº 312284.

ABBREVIATIONS

BPTCA, biphenyl-3,4',5-tricarboxylic acid; IPA, isophthalic acid; MOF, metal-organic framework; NEXAFS, near edge X-ray absorption fine structure; STM, scanning tunneling microscopy; TMA, trimesic acid; XPS, X-ray photoelectron spectroscopy.

REFERENCES

1. Rowsell, J. L. C.; Yaghi, O. M. Metal–Organic Frameworks: A New Class of Porous Materials. *Microporous Mesoporous Mater.* **2004**, *73*, 3-14.

2. Clair, S.; Pons, S.; Seitsonen, A. P.; Brune, H.; Kern, K.; Barth, J. V. Stm Study of Terephthalic Acid Self-Assembly on Au(111): Hydrogen-Bonded Sheets on an Inhomogeneous Substrate. *J. Phys. Chem. B* **2004**, *108*, 14585-14590.

3. Zhu, N.; Osada, T.; Komeda, T. Supramolecular Assembly of Biphenyl Dicarboxylic Acid on Au(111). *Surf. Sci.* **2007**, *601*, 1789-1794.

4. Pei, Z.; Lin, L.; Zhang, H.; Zhang, L.; Xie, Z. Self-Assembly of 2,6-Naphthalenedicarboxylic Acid and 4,4 '-Biphenyldicarboxylic Acid on Highly Oriented Pyrolytic Graphite and Au(1 1 1) Surfaces. *Electrochim. Acta* **2010**, *55*, 8287-8292.

5. Xiao, W. D.; Jiang, Y. H.; Aiet-Mansour, K.; Ruffieux, P.; Gao, H. J.; Fasel, R. Chiral Biphenyldicarboxylic Acid Networks Stabilized by Hydrogen Bonding. *J. Phys. Chem. C* **2010**, *114*, 6646-6649.

6. Shekhah, O.; Wang, H.; Kowarik, S.; Schreiber, F.; Paulus, M.; Tolan, M.; Sternemann, C.; Evers, F.; Zacher, D.; Fischer, R. A. et al. Step-by-Step Route for the Synthesis of Metal−Organic Frameworks. *J. Am. Chem. Soc.* **2007**, *129*, 15118-15119.

7. Zacher, D.; Shekhah, O.; Wöll, C.; Fischer, R. A. Thin Films of Metal-Organic Frameworks. *Chem. Soc. Rev.* **2009**, *38*, 1418-1429.

8. Shekhah, O.; Wang, H.; Zacher, D.; Fischer, R. A.; Wöll, C. Growth Mechanism of Metal–Organic Frameworks: Insights into the Nucleation by Employing a Step-by-Step Route. *Angew. Chem. Int. Ed.* **2009**, *48*, 5038-5041.

9. Tekiel, A.; Prauzner-Bechcicki, J. S.; Godlewski, S.; Budzioch, J.; Szymonski, M. Self-Assembly of Terephthalic Acid on Rutile Tio2(110): Toward Chemically Functionalized Metal Oxide Surfaces. *J. Phys. Chem. C* **2008**, *112*, 12606-12609.

10. Rahe, P.; Nimmrich, M.; Kuhnle, A. Substrate Templating Upon Self-Assembly of Hydrogen-Bonded Molecular Networks on an Insulating Surface. *Small* **2012**, *8*, 2969-2977.

11. Stepanow, S.; Lin, N.; Vidal, F.; Landa, A.; Ruben, M.; Barth, J. V.; Kern, K. Programming Supramolecular Assembly and Chirality in Two-Dimensional Dicarboxylate Networks on a Cu(100) Surface. *Nano Lett.* **2005**, *5*, 901-904.

12. Martin, D. S.; Cole, R. J.; Haq, S. Creating a Functionalized Surface: The Adsorption of Terephthalic Acid onto Cu(110). *Phys. Rev. B* **2002**, *66*.

13. Dmitriev, A.; Lin, N.; Weckesser, J.; Barth, J. V.; Kern, K. Supramolecular Assemblies of Trimesic Acid on a Cu(100) Surface. *J. Phys. Chem. B* **2002**, *106*, 6907-6912.

14. Frederick, B. G.; Chen, Q.; Leibsle, F. M.; Lee, M. B.; Kitching, K. J.; Richardson, N. V. Long-Range Periodicity in C(8x2) Benzoate/Cu(110): A Combined Stm, Leed and Hreels Study. *Surf. Sci.* **1997**, *394*, 1-25.

15. Stepanow, S.; Strunskus, T.; Lingenfelder, M.; Dmitriev, A.; Spillmann, H.; Lin, N.; Barth, J. V.; Wöll, C.; Kern, K. Deprotonation-Driven Phase Transformations in Terephthalic Acid Self-Assembly on Cu(100). *J. Phys. Chem. B* **2004**, *108*, 19392-19397.

16. Chen, Q.; Perry, C. C.; Frederick, B. G.; Murray, P. W.; Haq, S.; Richardson, N. V. Structural Aspects of the Low-Temperature Deprotonation of Benzoic Acid on Cu(110) Surfaces. *Surf. Sci.* **2000**, *446*, 63-75.

17. Classen, T.; Lingenfelder, M.; Wang, Y.; Chopra, R.; Virojanadara, C.; Starke, U.; Costantini, G.; Fratesi, G.; Fabris, S.; de Gironcoli, S. et al. Hydrogen and Coordination Bonding Supramolecular Structures of Trimesic Acid on Cu(110). *J. Phys. Chem. A* **2007**, *111*, 12589-12603.

18. Ge, Y.; Adler, H.; Theertham, A.; Kesmodel, L. L.; Tait, S. L. Adsorption and Bonding of First Layer and Bilayer Terephthalic Acid on the Cu(100) Surface by High-Resolution Electron Energy Loss Spectroscopy. *Langmuir* **2010**, *26*, 16325-16329.

19. Canas-Ventura, M. E.; Klappenberger, F.; Clair, S.; Pons, S.; Kern, K.; Brune, H.; Strunskus, T.; Woell, C.; Fasel, R.; Barth, J. V. Coexistence of One- and Two-Dimensional Supramolecular Assemblies of Terephthalic Acid on Pd(111) Due to Self-Limiting Deprotonation. *J. Chem. Phys.* **2006**, *125*.

20. Payer, D.; Comisso, A.; Dmitriev, A.; Strunskus, T.; Lin, N.; Woell, C.; DeVita, A.; Barth, J. V.; Kern, K. Ionic Hydrogen Bonds Controlling Two-Dimensional Supramolecular Systems at a Metal Surface. *Chem. Eur. J.* **2007**, *13*, 3900-3906.

21. Schwarz, D.; van Gastel, R.; Zandvliet, H. J. W.; Poelsema, B. In Situ Observation of a Deprotonation-Driven Phase Transformation: 4,4 '-Biphenyldicarboxylic Acid on Au(111). *J. Phys. Chem. C* **2013**, *117*, 1020-1029.

22. Ruben, M.; Payer, D.; Landa, A.; Comisso, A.; Gattinoni, C.; Lin, N.; Collin, J.-P.; Sauvage, J.-P.; De Vita, A.; Kern, K. 2d Supramolecular Assemblies of Benzene-1,3,5-Triyl-Tribenzoic Acid: Temperature-Induced Phase Transformations and Hierarchical Organization with Macrocyclic Molecules. *J. Am. Chem. Soc.* **2006**, *128*, 15644-15651.

23. Lin, N.; Payer, D.; Dmitriev, A.; Strunskus, T.; Wöll, C.; Barth, J. V.; Kern, K. Two-Dimensional Adatom Gas Bestowing Dynamic Heterogeneity on Surfaces. *Angew. Chem. Int. Ed.* **2005**, *44*, 1488-1491.

24. Suzuki, T.; Lutz, T.; Payer, D.; Lin, N.; Tait, S. L.; Costantini, G.; Kern, K. Substrate Effect on Supramolecular Self-Assembly: From Semiconductors to Metals. *Phys. Chem. Chem. Phys.* **2009**, *11*, 6498-6504.

25. Kley, C. S.; Cechal, J.; Kumagai, T.; Schramm, F.; Ruben, M.; Stepanow, S.; Kern, K. Highly Adaptable Two-Dimensional Metal-Organic Coordination Networks on Metal Surfaces. *J. Am. Chem. Soc.* **2012**, *134*, 6072-6075.

26. Clair, S.; Pons, S.; Fabris, S.; Baroni, S.; Brune, H.; Kern, K.; Barth, J. V. Monitoring Two-Dimensional Coordination Reactions: Directed Assembly of Co-Terephthalate Nanosystems on Au(111). *J. Phys. Chem. B* **2006**, *110*, 5627-5632.

27. Zhang, Y.-F.; Zhu, N.; Komeda, T. Programming of a Mn-Coordinated 4-4′-Biphenyl Dicarboxylic Acid Nanosystem on Au(111) and Investigation of the Non-Covalent Binding of C60 Molecules. *Surf. Sci.* **2008**, *602*, 614-619.

28. Ishikawa, Y.; Ohira, A.; Sakata, M.; Hirayama, C.; Kunitake, M. A Two-Dimensional Molecular Network Structure of Trimesic Acid Prepared by Adsorption-Induced Self-Organization. *Chem. Commun.* **2002**, 2652-2653.

29. De Feyter, S.; Gesquiere, A.; Klapper, M.; Mullen, K.; De Schryver, F. C. Toward Two-Dimensional Supramolecular Control of Hydrogen-Bonded Arrays: The Case of Isophthalic Acids. *Nano Lett.* **2003**, *3*, 1485-1488.

30. Duong, A.; Dubois, M.-A.; Wuest, J. D. Two-Dimensional Molecular Organization of Pyridinecarboxylic Acids Adsorbed on Graphite. *Langmuir* **2010**, *26*, 18089-18096.

31. Zhou, H.; Maris, T.; Wuest, J. D. Using Systematic Comparisons of 2d and 3d Structures to Reveal Principles of Molecular Organization. Tetraesters of Linear Bisisophthalic Acids. *J. Phys. Chem. C* **2012**, *116*, 13052-13062.

32. Stannard, A.; Russell, J. C.; Blunt, M. O.; Salesiotis, C.; Gimenez-Lopez, M. D.; Taleb, N.; Schroder, M.; Champness, N. R.; Garrahan, J. P.; Beton, P. H. Broken Symmetry and the

Variation of Critical Properties in the Phase Behaviour of Supramolecular Rhombus Tilings. *Nat. Chem.* **2012**, *4*, 112-117.

33. Blunt, M. O.; Russell, J. C.; Gimenez-Lopez, M. D.; Garrahan, J. P.; Lin, X.; Schroder, M.; Champness, N. R.; Beton, P. H. Random Tiling and Topological Defects in a Two-Dimensional Molecular Network. *Science* **2008**, *322*, 1077-1081.

34. Lackinger, M.; Heckl, W. M. Carboxylic Acids: Versatile Building Blocks and Mediators for Two-Dimensional Supramolecular Self-Assembly. *Langmuir* **2009**, *25*, 11307-11321.

35. Kampschulte, L.; Werblowsky, T. L.; Kishore, R. S. K.; Schmittel, M.; Heckl, W. M.; Lackinger, M. Thermodynamical Equilibrium of Binary Supramolecular Networks at the Liquid-Solid Interface. *J. Am. Chem. Soc.* **2008**, *130*, 8502-8507.

36. Kim, B. I.; Hanson, J.; Turner, M.; Reeder, L. Influence of Solvent on the Chiral Resolution of Organic Molecules on Au(111): Ec-Stm Study of Biphenyl Dicarboxylic Acid on Au(111) in an Aqueous Environment. *Surf. Sci.* **2012**, *606*, 1340-1344.

37. Cebula, I.; Smith, E. F.; Gimenez-Lopez, M. d. C.; Yang, S.; Schröder, M.; Champness, N. R.; Beton, P. H. Packing of Isophthalate Tetracarboxylic Acids on Au(111): Rows and Disordered Herringbone Structures. *J. Phys. Chem. C* **2013**, *117*, 18381-18385.

38. Wasio, N. A.; Quardokus, R. C.; Forrest, R. P.; Lent, C. S.; Corcelli, S. A.; Christie, J. A.; Henderson, K. W.; Kandel, S. A. Self-Assembly of Hydrogen-Bonded Two-Dimensional Quasicrystals. *Nature* **2014**, *507*, 86-89.

39. Tao, Y. T.; Lee, M. T.; Chang, S. C. Effect of Biphenyl and Naphthyl Groups on the Structure of Self-Assembled Monolayers - Packing, Orientation, and Wetting Properties. *J. Am. Chem. Soc.* **1993**, *115*, 9547-9555.

40. Tao, Y. T.; Huang, C. Y.; Chiou, D. R.; Chen, L. J. Infrared and Atomic Force Microscopy Imaging Study of the Reorganization of Self Assembled Monolayers of Carboxylic Acids on Silver Surface. *Langmuir* **2002**, *18*, 8400-8406.

41. Cebula, I.; Lu, H.; Zharnikov, M.; Buck, M. Monolayers of Trimesic and Isophthalic Acid on Cu and Ag: The Influence of Coordination Strength on Adsorption Geometry. *Chem. Sci.* **2013**, *4*, 4455-4464.

42. Cebula, I.; Shen, C.; Buck, M. Isophthalic Acid: A Basis for Highly Ordered Monolayers. *Angew. Chem. Int. Ed.* **2010**, *49*, 6220-6223.

43. Shen, C.; Cebula, I.; Brown, C.; Zhao, J.; Zharnikov, M.; Buck, M. Structure of Isophthalic Acid Based Monolayers and Its Relation to the Initial Stages of Growth of Metal-Organic Coordination Layers. *Chem. Sci.* **2012**, *3*, 1858-1865.

44. Han, B.; Li, Z.; Wandlowski, T. Adsorption and Self-Assembly of Aromatic Carboxylic Acids on Au/Electrolyte Interfaces. *Anal. Biolanal. Chem.* **2007**, *388*, 121-129.

45. Su, G. J.; Zhang, H. M.; Wan, L. J.; Bai, C. L.; Wandlowski, T. Potential-Induced Phase Transition of Trimesic Acid Adlayer on Au(111). *J. Phys. Chem. B* **2004**, *108*, 1931-1937.

46. Li, Z.; Han, B.; Wan, L. J.; Wandlowski, T. Supramolecular Nanostructures of 1,3,5-Benzene-Tricarboxylic Acid at Electrified Au(111)/0.05 M H2so4 Interfaces: An in Situ Scanning Tunneling Microscopy Study. *Langmuir* **2005**, *21*, 6915-6928.

47. Zelenay, P.; Waszczuk, P.; Dobrowolska, K.; Sobkowski, J. Adsorption of Benzoic-Acid on a Polycrystalline Gold Electrode. *Electrochim. Acta* **1994**, *39*, 655-660.

48. Wong-Foy, A. G.; Lebel, O.; Matzger, A. J. Porous Crystal Derived from a Tricarboxylate Linker with Two Distinct Binding Motifs. *J. Am. Chem. Soc.* **2007**, *129*, 15740-15741.

49. Lim, C.-S.; Schnobrich, J. K.; Wong-Foy, A. G.; Matzger, A. J. Metal-Dependent Phase Selection in Coordination Polymers Derived from a C-2v-Symmetric Tricarboxylate. *Inorg. Chem.* **2010**, *49*, 5271-5275.

50. Li, L.; Luo, J.; Wang, S.; Sun, Z.; Chen, T.; Hong, M. A Unique Independent One-Dimensional Green Luminescent Coordination Polymer Nanotube Based on an Unsymmetric Tricarboxylate Linker. *Crystal Growth & Design* **2011**, *11*, 3744-3747.

51. Lu, Y.; Zhao, W.; Liu, Y.; Liu, B.; Feng, X.; Tan, J.; Li, X.; Yang, X. Crystal Structures, Fluorescent and Magnetic Properties of Five New Coordination Polymers Based on Biphenyl-3,4 ',5-Tricarboxylic Acid. *J. Solid State Chem.* **2012**, *192*, 144-152.

52. Liu, T.; Wang, S.; Lu, J.; Dou, J.; Niu, M.; Li, D.; Bai, J. Positional Isomeric and Substituent Effect on the Assemblies of a Series of D10 Coordination Polymers Based Upon Unsymmetric Tricarboxylate Acids and Nitrogen-Containing Ligands. *CrystEngComm* **2013**, *15*, 5476-5489.

53. Li, L.; Zhang, S.; Han, L.; Sun, Z.; Luo, J.; Hong, M. A Non-Centrosymmetric Dual-Emissive Metal-Organic Framework with Distinct Nonlinear Optical and Tunable Photoluminescence Properties. *Crystal Growth & Design* **2013**, *13*, 106-110.

54. Zhang, X.; Fan, L.; Zhang, W.; Fan, W.; Sun, L.; Zhao, X. Syntheses, Structures, and Magnetic Properties of Five Coordination Polymers Constructed from Biphenyl-3,4',5-Tricarboxylic Acid and (Bis)Imidazole Linkers. *CrystEngComm* **2014**, *16*, 3203-3213.

55. Chen, X.; Tong, Y.; Han, M.-M.; Cao, K.-L.; Feng, Y.-L. Two Luminescent Metal - Organic Frameworks Constructed by Unsymmetric Tricarboxylate. *Inorg. Chem. Commun.* **2014**, *40*, 62-65.

56. Kondo, T.; Morita, J.; Okamura, M.; Saito, T.; Uosaki, K. In Situ Structural Study on Underpotential Deposition of Ag on Au(111) Electrode Using Surface X-Ray Scattering Technique. *J. Electroanal. Chem.* **2002**, *532*, 201-205.

57. Kondo, T.; Takakusagi, S.; Uosaki, K. Stability of Underpotentially Deposited Ag Layers on a Au(111) Surface Studied by Surface X-Ray Scattering. *Electrochem. Commun.* **2009**, *11*, 804-807.

58. Chen, C. H.; Vesecky, S. M.; Gewirth, A. A. Insitu Atomic Force Microscopy of Underpotential Deposition of Ag on Au(111). *J. Am. Chem. Soc.* **1992**, *114*, 451-458.

59. Hotlos, J.; Magnussen, O. M.; Behm, R. J. Effect of Trace Amounts of Cl− in Cu Underpotential Deposition on Au(111) in Perchlorate Solutions: An in-Situ Scanning Tunneling Microscopy Study. *Surf. Sci.* **1995**, *335*, 129-144.

60. Wu, S.; Lipkowski, J.; Tyliszczak, T.; Hitchcock, A. P. Effect of Anion Adsorption on Early Stages of Copper Electrocrystallization at Au(111) Surface. *Prog. Surf. Sci.* **1995**, *50*, 227-236.

61. Herrero, E.; Buller, L. J.; Abruña, H. D. Underpotential Deposition at Single Crystal Surfaces of Au, Pt, Ag and Other Materials. *Chem. Rev.* **2001**, *101*, 1897-1930.

62. Moulder, J. F.; Stickle, W. E.; Sobol, P. E.; Bomben, K. D. *Handbook of X-Ray Photoelectron Spectroscopy*; Perkin-Elmer Corp. : Eden Prairie, MN, 1992.

63. Stöhr, J. *Nexafs Spectroscopy*; Springer, 1992.

64. Batson, P. E. Carbon 1s near-Edge-Absorption Fine Structure in Graphite. *Phys. Rev. B* **1993**, *48*, 2608-2610.

65. Frisch, M. J.; Trucks, G. W.; Schlegel, H. B.; Scuseria, G. E.; Robb, M. A.; Cheeseman, J. R.; Zakrzewski, V. G.; Montgomery, J. A.; Stratmann, R. E.; Burant, J. C. et al. *Gaussian 98 (Rev. A.7)*; Gaussian, Inc.: Pittsburgh, PA, 1998.

66. Batina, N.; Will, T.; Kolb, D. M. Study of the Initial-Stages of Copper Deposition by in-Situ Scanning-Tunneling-Microscopy. *Faraday Discuss.* **1992**, 93-106.

67. Schneeweiss, M. A.; Kolb, D. M. The Initial Stages of Copper Deposition on Bare and Chemically Modified Gold Electrodes. *Phys. Stat. Sol. A* **1999**, *173*, 51-71.

68. Geyer, W.; Stadler, V.; Eck, W.; Zharnikov, M.; Gölzhäuser, A.; Grunze, M. Electron-Induced Crosslinking of Aromatic Self-Assembled Monolayers: Negative Resists for Nanolithography. *Appl. Phys. Lett.* **1999**, *75*, 2401-2403.

69. Heister, K.; Rong, H. T.; Buck, M.; Zharnikov, M.; Grunze, M.; Johansson, L. S. O. Odd-Even Effects at the S-Metal Interface and in the Aromatic Matrix of Biphenyl-Substituted Alkanethiol Self-Assembled Monolayers. *J. Phys. Chem. B* **2001**, *105*, 6888-6894.

70. Frey, S.; Stadler, V.; Heister, K.; Eck, W.; Zharnikov, M.; Grunze, M.; Zeysing, B.; Terfort, A. Structure of Thioaromatic Self-Assembled Monolayers on Gold and Silver. *Langmuir* **2001**, *17*, 2408-2415.

71. Küller, A.; Eck, W.; Stadler, V.; Geyer, W.; Gölzhäuser, A. Nanostructuring of Silicon by Electron-Beam Lithography of Self-Assembled Hydroxybiphenyl Monolayers. *Appl. Phys. Lett.* **2003**, *82*, 3776-3778.

72. Zharnikov, M. High-Resolution X-Ray Photoelectron Spectroscopy in Studies of Self-Assembled Organic Monolayers. *J. Electron. Spectrosc. Relat. Phenom.* **2010**, *178*, 380-393.

73. Dmitriev, A.; Spillmann, H.; Stepanow, S.; Strunskus, T.; Woll, C.; Seitsonen, A. P.; Lingenfelder, M.; Lin, N.; Barth, J. V.; Kern, K. Asymmetry Induction by Cooperative Intermolecular Hydrogen Bonds in Surface-Anchored Layers of Achiral Molecules. *ChemPhysChem* **2006**, *7*, 2197-2204.

74. Wühn, A.; Weckesser, J.; Wöll, C. Bonding and Orientational Ordering of Long-Chain Carboxylic Acids on Cu(111): Investigations Using X-Ray Absorption Spectroscopy. *Langmuir* **2001**, *17*, 7605-7612.

75. Zharnikov, M.; Frey, S.; Heister, K.; Grunze, M. An Extension of the Mean Free Path Approach to X-Ray Absorption Spectroscopy. *J. Electron. Spectrosc. Relat. Phenom.* **2002**, *124*, 15-24.

76. Schreiber, F. Structure and Growth of Self-Assembling Monolayers. *Prog. Surf. Sci.* **2000**, *65*, 151-256.

77. Cyganik, P.; Buck, M.; Azzam, W.; Wöll, C. Self-Assembled Monolayers of Ω-Biphenyl-Alkane Thiols on Au(111): Influence of Spacer Chain on Molecular Packing. *J. Phys. Chem. B* **2004**, *108*, 4989-4996.

78. Kreikemeyer-Lorenzo, D.; Unterberger, W.; Duncan, D. A.; Bradley, M. K.; Lerotholi, T. J.; Robinson, J.; Woodruff, D. P. Face-Dependent Bond Lengths in Molecular Chemisorption: The Formate Species on Cu(111) and Cu(110). *Phys. Rev. Lett.* **2011**, *107*, 046102.

79. Rodriguez-Cuamatzi, P.; Arillo-Flores, O. I.; Bernal-Urucurtu, M. I.; Hoepfl, H. Experimental and Theoretical Analysis of the Hydrogen-Bonding Motifs Formed between the Carboxyl and the Carboxylate Classification of Group: Towards a Systematic Their Supramolecular Motifs. *Supramol. Chem.* **2007**, *19*, 559-578.

80. Han, P.; Kurland, A. R.; Giordano, A. N.; Nanayakkara, S. U.; Blake, M. M.; Pochas, C. M.; Weiss, P. S. Heads and Tails: Simultaneous Exposed and Buried Interface Imaging of Monolayers. *Acs Nano* **2009**, *3*, 3115-3121.

81. Qi, Y.; Yaffe, O.; Tirosh, E.; Vilan, A.; Cahen, D.; Kahn, A. Filled and Empty States of Alkanethiol Monolayer on Au (111): Fermi Level Asymmetry and Implications for Electron Transport. *Chem. Phys. Lett.* **2011**, *511*, 344-347.

82. Yaffe, O.; Qi, Y.; Scheres, L.; Puniredd, S. R.; Segev, L.; Ely, T.; Haick, H.; Zuilhof, H.; Vilan, A.; Kronik, L. et al. Charge Transport across Metal/Molecular (Alkyl) Monolayer-Si Junctions Is Dominated by the Lumo Level. *Phys. Rev. B* **2012**, *85*, 045433.